

**1 Dependence of entrainment in shallow cumulus**  
**2 convection on vertical velocity and distance to cloud**  
**3 edge**

Yang Tian,<sup>1</sup> Zhiming Kuang<sup>1,2</sup>

---

Corresponding author: Yang Tian. Department of Earth and Planetary Sciences, Harvard University, Cambridge, Massachusetts, USA. (yangtian@fas.harvard.edu)

<sup>1</sup>Department of Earth and Planetary Sciences, Harvard University, Cambridge, Massachusetts, USA.

<sup>2</sup>John A. Paulson School of Engineering and Applied Sciences, Harvard University, Cambridge, Massachusetts, USA.

4 The dependence of entrainment rate on environmental conditions and cloud  
5 characteristics is investigated using large-eddy simulations (LES) of the re-  
6 sponse of shallow cumulus convection to a small-amplitude temperature per-  
7 turbation that is horizontally uniform and localized in height. The simulated  
8 cumulus fields are analyzed in the framework of an ensemble of entraining  
9 plumes by tracking a large number of Lagrangian parcels embedded in the  
10 LES and grouping them into different plumes based on their detrainment height.  
11 The results show that fractional entrainment rate per unit height of a plume  
12 is inversely proportional to its vertical velocity and its distance to the cloud  
13 edge, while changes in environmental stratification and relative humidity, the  
14 plume's buoyancy, or the vertical gradient of its buoyancy due to the tem-  
15 perature perturbation have little effect on the plume's entrainment rate.

## 1. Introduction

16 How entrainment processes in cumulus clouds depend on environmental conditions and  
17 cloud characteristics has been an active area of research, and choices of such dependence  
18 in cumulus parameterization schemes are highly consequential to the schemes' behavior  
19 and the simulated large-scale weather and climate [e.g. *Grant and Brown*, 1999; *Gregory*,  
20 2001; *Neggers et al.*, 2002; *Bechtold et al.*, 2008; *Chikira and Sugiyama*, 2010; *Mapes and*  
21 *Neale*, 2011; *Dawe and Austin*, 2013].

22 In discussing entrainment, it is important to specify the conceptual model, within  
23 which entrainment is defined. The most widely used models include the bulk entraining-  
24 detraining plume model, where the cumulus ensemble is represented by a single bulk  
25 plume [e.g. *Tiedtke*, 1989], and the spectral entraining plume ensemble model, where  
26 the cumulus ensemble is represented by a spectrum of entraining plumes with different  
27 entrainment characteristics [e.g. *Arakawa and Schubert*, 1974], as well as different formu-  
28 lations of multi-parcel models [e.g. *Raymond and Blyth*, 1986; *Nie and Kuang*, 2012a;  
29 *Neggers et al.*, 2002]. Drawing from theories of similarity plumes such as *Morton et al.*  
30 [1956], an inverse relationship between the fractional entrainment rate per unit height <sup>1</sup>  
31  $\epsilon = d \ln(M)/dz$  (where  $M$  is the mass flux and  $z$  is height) and cloud size  $R$ , i.e.  $\epsilon \propto \frac{1}{R}$ ,  
32 has been often used in bulk entraining-detraining plume models [e.g. *Simpson and Wig-*  
33 *gert*, 1969; *Tiedtke*, 1989; *Siebesma*, 1998; *Bretherton et al.*, 2004]. As cloud size tends to  
34 be larger for deeper clouds, some authors have proposed, again in the context of a bulk  
35 entraining-detraining plume model, to tie  $\epsilon$  to the height of the cloud, as  $\epsilon \propto 1/z$  [e.g.  
36 *Siebesma*, 1998] or with other empirically fitted formulae [*Hohenegger and Bretherton*,

2011]. *Neggers et al.* [2002] suggested that in their multiple-parcel model,  $\epsilon$  of a parcel is  
inversely proportional to the parcel's vertical velocity. This formulation is further applied  
to a spectral entraining plume ensemble model by *Chikira and Sugiyama* [2010]. There  
are also ideas that relate  $\epsilon$  to thermodynamical properties: based on earlier modeling  
work by *Bretherton and Smolarkiewicz* [1989], *Emanuel and Zivkovic-Rothman* [1999] ar-  
gued in general terms that entrainment should increase with increasing vertical gradient  
of cloud buoyancy ( $db/dz$ , where  $b$  is the cloud buoyancy) because of the inflow associated  
with such a gradient, whereas *Lin* [1999] suggested that within an ensemble of entraining  
plumes, plumes with smaller buoyancy have larger entrainment rates, and *Bechtold et*  
*al.* [2008] suggested that in the context of a bulk entraining-detraining plume model,  $\epsilon$   
increases with decreasing environmental relative humidity. *Gregory* [2001] suggested a  
formulation where the entrainment rate of a bulk plume is proportional to its buoyancy  
and inversely proportional to the square of its vertical velocity. This formulation was  
further used in an entraining plume ensemble model by *Chikira and Sugiyama* [2010].

While the above ideas all drew inspiration from numerical simulations and theoretical  
reasoning, adequate support for these ideas has been lacking. *Romps* [2010] tested some  
of these ideas in the context of a bulk entraining-detraining plume model and did not  
find evidence for the  $\epsilon \propto 1/z$  relationship or any simple relationship between  $\epsilon$  and  $b$ , or  
 $\epsilon$  and  $db/dz$ , although it is worth noting that he calculated entrainment and detrainment  
rates by tracking grid boxes moving in and out of the cloudy updraft category so that  
his definition of bulk entrainment and detrainment rates differs from the more commonly  
used effective bulk entrainment and detrainment rates.

59 One difficulty with diagnosing the relationship between fractional entrainment rate and  
60 potential contributing factors, as with all statistical inference, is the effect of confounding:  
61 multiple factors can contribute and interfere, making causal inference difficult. To reduce  
62 the extent of confounding, we analyze changes in entrainment in response to a small-  
63 amplitude temperature perturbation that is horizontally uniform and localized in height.  
64 With such a linear response function approach [*Kuang, 2010*], we can identify changes in  
65 entrainment characteristics associated with changes in specific environmental conditions,  
66 while minimizing changes in other environmental conditions as well as changes in cloud  
67 characteristics unrelated to the imposed perturbation. This helps to reduce the extent of  
68 (but does not eliminate) confounding and allows for more definitive inferences.

69 The analysis in this paper will be in the framework of an ensemble of entraining plumes  
70 of *Arakawa and Schubert* [1974], where plumes are distinguished by their detrainment  
71 heights and experience only entrainment (no detrainment) before detrainment. Here the  
72 fractional entrainment rates are diagnosed and vary with height instead of being constant  
73 in height as assumed in *Arakawa and Schubert* [1974]. We also note that the entraining  
74 plume ensembles can be combined to give a bulk entraining-detraining plume [see e.g.  
75 *Lawrence and Rasch, 2005*].

76 Casting the numerically simulated cumulus ensemble in terms of an ensemble of en-  
77 training plumes is achieved by tracking Lagrangian particles embedded in large-eddy  
78 simulations (LES), similar to *Lin and Arakawa* [1997]. The term "entraining plumes" is  
79 used here as a way of grouping cloudy updraft parcels in a statistical sense, and they  
80 should not be viewed as physical structures such as the similarity plumes in the water

81 tank experiments. Therefore, a "plume" here is a collection of air parcels from different  
82 clouds, and parcels from a single cloud contribute to multiple "plumes".

83 We will focus on non-precipitating shallow cumuli in this paper. Without the complicat-  
84 ing processes associated with precipitation, shallow cumuli are an excellent starting point  
85 for studying the cumulus entrainment process. Applications of the present methodology  
86 to deep convection will be described in a forthcoming paper.

87 Section 2 describes the model used and the experimental design. The method of anal-  
88 ysis, the results, and their interpretations are presented in section 3, followed by a brief  
89 summary in section 4.

## 2. Models and experimental design

90 The Large Eddy Simulations (LES) were performed with the System for Atmospheric  
91 Modeling (SAM) version 6.8.2 [*Khairoutdinov and Randall, 2001*] for the undisturbed  
92 phase of the Barbados Oceanographic and Meteorological Experiment (BOMEX) [*Holland  
93 and Rasmusson, 1973*]. SAM was run with a doubly periodic domain (6.4km x 6.4km) and  
94 a horizontal grid spacing of 50m. There are 128 vertical layers with a 25m grid spacing.  
95 The time step is 1s. A monotonic advection scheme is used for scalars and the subgrid-  
96 scale turbulent fluxes are determined using a 1.5 order closure scheme. The experimental  
97 settings of this BOMEX case, such as the initial soundings, the large-scale forcing, and  
98 surface fluxes, are the same as those used in *Siebesma et al. [2003]*.

99 We first ran the model for 6 hours, with the first 3 hours discarded as spin-up. Starting  
100 from the end of the 3rd hour, restart files were output every 5 minutes. A set of 30-  
101 minute long simulations were initialized from these restart files but with a temperature

102 perturbation added to the initial conditions. The temperature perturbation is horizontally  
103 uniform, Gaussian-shaped in height, centered at 975m with a half-width of 75m and a  
104 peak value of +0.25K (Fig. 1). This set of simulations, combined with the initial 6-hour  
105 long simulation, provides 36 pairs of 30-minute long control and perturbed runs in which  
106 the perturbed runs start from the same fully developed cumulus fields as the control  
107 runs except with the added temperature perturbation. The averaged differences between  
108 these pairs of runs are taken as the convective responses to the imposed temperature  
109 perturbation. As convection responds to the temperature anomaly, the amplitude of the  
110 initially added temperature anomaly roughly halves over the half hour of simulation, and  
111 some moisture anomalies start to develop (Fig. 1), similar to *Nie and Kuang* [2012a].  
112 The 30-minute simulation length was chosen to allow clouds enough time to respond to  
113 the imposed temperature perturbation, yet is short enough so that averaged over this  
114 time period, the main difference between the horizontally averaged profiles of the control  
115 and perturbed experiments remains to be a temperature anomaly localized in height.  
116 In future studies, we will impose time-invariant temperature and moisture tendencies to  
117 further reduce the evolution of the initially imposed perturbation.

118 To aid our analysis, we embed a Lagrangian Parcel Dispersion Model (LPDM) into  
119 the LES as in *Nie and Kuang* [2012b]. It releases 1600 passive parcels inside each LES  
120 vertical column (totaling more than 30 million particles in the LES domain) and advects  
121 them based on the LES resolved winds. The release positions of the parcels have a  
122 random uniform probability distribution in the horizontal as well as in pressure up to the  
123 2500m vertical level. Combining the trajectories of the parcels with the snapshots of the

124 LES output provides a full history of parcel properties along their trajectories, thus a  
125 Lagrangian perspective on cumulus scale dynamics [e.g. *Weil, 2004; Heus, 2008; Nie and*  
126 *Kuang, 2012b; Yeo and Romps, 2013; Torri et al., 2015*]. Some basic validations of the  
127 LPDM are included in the online supplementary material.

### 3. Analysis and Results

#### a. Response to the temperature perturbation

128 We shall view the simulated cumulus field in the framework of an ensemble of entraining  
129 plumes as in, e.g., *Lin and Arakawa [1997]* and *Kuang and Bretherton [2006]*. Grid boxes  
130 are considered cloudy updrafts if they have vertical velocities greater than 1m/s and non-  
131 precipitating liquid water mixing ratios greater than 0.01g/kg. We then identify grid  
132 boxes at 612.5m, which is just above the cloud base, that are cloudy updrafts and track  
133 all parcels within these grid boxes (there are 20 parcels per grid box) until they detrain,  
134 where detrainment is defined as parcels exiting cloudy updrafts and not reentering within  
135 1 minute [*Nie and Kuang, 2012b*]. We then sort these cloudy updraft parcels that detrain  
136 above 762.5m into 100 groups based on their detrainment heights. For example, among  
137 all cloudy updraft parcels that are from 612.5m and detrain above 762.5m, the 1 % of  
138 the parcels that detrain at the highest levels are grouped together as one parcel group  
139 (or plume), then the next highest 1% and so on, totaling 100 parcel groups, with larger  
140 group numbers indicating higher detrainment heights. The relatively large vertical velocity  
141 threshold, compared to, e.g., *Nie and Kuang [2012a]* was chosen to exclude gravity-wave  
142 generated vertical fluctuations. Changing the time interval to a longer period (2 min, 3  
143 min, 4 min or 5 min) does not change the general results. A detrainment height of 762.5m



144 or higher is imposed to reduce the number of parcels that need to be tracked, as many  
145 cloudy updraft parcels from the cloud base detrain at very low altitudes. We will use  
146 the terms "parcel group" and "plume" interchangeably as parcel grouping is our way of  
147 defining the plumes in the plume ensemble model. Note that the parcel groups defined  
148 here were also referred to as subensembles in the literature [e.g. *Lin and Arakawa, 1997*].

149 With the above definition of parcel groups, we can determine the height range over  
150 which the parcels of a particular parcel group detrain (the range can be different between  
151 the control and the perturbed experiments). We then identify all cloudy updraft parcels  
152 that detrain over this height range (not just those originate from the cloud base). Those  
153 parcels that do not originate from the cloud base level are said to have been entrained  
154 between the cloud base and their detrainment height. The height of entrainment for a  
155 parcel is determined as the height at which the parcel enters a cloudy updraft and does not  
156 exit within 1 minute. The fractional entrainment rate as a function of height is calculated  
157 as the fractional increase in the mass flux carried by all parcels in this parcel group per  
158 unit increase in height. Again, the results are not sensitive to the choice of the 1-min time  
159 interval.

160 In addition to properties such as buoyancy, vertical velocity, and total water, we also  
161 compute the minimum distance to the cloud edge for each of the grid boxes within the  
162 cloudy updraft. The cloud edge is defined to be the horizontal boundary between grid  
163 boxes that are cloudy (liquid water greater than 0.01g/kg) and those that are not. Prop-  
164 erties of a parcel are set to be those of the grid box that it resides in (including distance  
165 to cloud edge), and properties of a parcel group are given by the averaged properties of

166 all parcels that detrain over the detrainment height range of that parcel group, including  
167 parcels originating from cloud base and those entrained later. The choice of a relatively  
168 large number (100) of parcel groups is meant to enhance, to some extent, homogene-  
169 ity within each group while exposing differences among the different groups. Given the  
170 chaotic nature of cumulus convection, it is not meaningful to track individual parcels in  
171 both control and perturbed runs and analyze changes in their behaviors due to the pertur-  
172 bation. Using our method of parcel grouping, parcels belonging to the same parcel group  
173 in the control and perturbed runs may be viewed as the same parcels in a statistical sense.

174 Fig. 2 shows parcel group properties in the control runs (Fig. 2a-e) and their changes in  
175 the perturbed runs relative to the control (Fig. 2f-j) as functions of parcel group number  
176 (x axis) and height (y axis). Figs. 2c and 2d show that buoyancy and total water content  
177 at the cloud base are uniform across the different parcel groups, while Figs. 2b and 2d  
178 show that a parcel that detrains higher tends to start at the cloud base slightly further  
179 away from the cloud edge and with slightly higher vertical velocity, indicating some roles  
180 of initial conditions in determining the fate of cloudy updrafts. Fig. 2e shows that parcel  
181 groups that reach higher tend to have smaller fractional entrainment rate. These parcels  
182 become increasingly more positively buoyant with higher vertical velocity during their  
183 ascent relative to those parcels that detrain at lower heights (smaller group numbers),  
184 which possess smaller positive buoyancy up to their detrainment levels. The vertical  
185 velocity of the highest reaching parcel groups can reach up to 4 m/s as they enter the  
186 base of the trade inversion (around 1500m). After that point, the buoyancy acceleration  
187 begins to decrease. Total water content decreases monotonically with height for all parcel

188 groups but more slowly for the higher-reaching ones. These results are consistent with  
189 those of *Romps and Kuang* [2010], who showed that in-cloud heterogeneity is mostly  
190 caused by the stochastic nature of the entrainment process, not the initial conditions at  
191 the cloud base. As such, their conclusion was that initial conditions at the cloud base have  
192 no *dominant control* on the fate of cloudy updrafts, but did not exclude the possibility  
193 that initial conditions at the cloud base can have some influence on the fate of cloudy  
194 updrafts. As discussed later in the next section, differences in entrainment rates among  
195 the different parcel groups near the cloud base likely come from the stochastic nature  
196 of the entrainment process, which implies that the different parcel groups are mostly a  
197 measure of how "lucky" the parcels are in avoiding dilution from entrainment.

198 We now focus on those parcel groups that are most affected by the added perturba-  
199 tion (parcel group 75 and higher) and examine their responses to the perturbation; the  
200 other parcel groups detrain at lower altitudes and do not experience the full effect of  
201 the added perturbation. The imposed warm anomaly forms a buoyancy barrier, shown  
202 as a belt of negative buoyancy anomalies in the perturbed layer (Fig. 2f). The change  
203 in vertical velocity (Fig. 2g) is consistent with that of buoyancy acceleration: updraft  
204 vertical velocity decreases inside and above the perturbed region with less reduction for  
205 the highest reaching parcels, which experience smaller buoyancy reduction because they  
206 traverse the barrier more quickly. In this non-precipitating shallow cumulus case, total  
207 water is a conserved quantity. The slight increase of total water content in the perturbed  
208 region and its decrease above is the result of changes in the entrainment. Overall, the  
209 results here are consistent with those in *Nie and Kuang* [2012a]. A full discussion of the

210 underlying mechanisms of these responses from a Lagrangian perspective will be presented  
211 in a separate paper. Below we shall focus on the entrainment process.

### **b. Dependence of entrainment on vertical velocity and distance to cloud edge**

212 Cloudy updrafts in the control and the perturbed cases have similar characteristics at  
213 the cloud base, as evidenced by the small differences at the cloud base seen in the right  
214 columns of Fig. 2. Above the cloud base, the cloudy updrafts entrain slightly less (per unit  
215 height) in the lower portion of the added temperature perturbation (one half width below  
216 the peak of the perturbation, or below  $\sim 900\text{m}$ ) and entrain more at higher altitudes in the  
217 perturbed runs (Fig. 2j). There are a number of ways that the warm anomaly may change  
218 the entrainment process. The warm anomaly increases the stratification below the peak  
219 of the perturbation and decreases it above, thus modifying the vertical gradient of cloud  
220 buoyancy which has been argued to be a control on entrainment [*Emanuel and Zivkovic-*  
221 *Rothman*, 1999]. The added warm anomaly also reduces cloud buoyancy (Fig. 2f) and  
222 environmental relative humidity, which were suggested by *Lin* [1999] and *Bechtold et al.*  
223 [2008], respectively, to enhance entrainment. Other factors that may contribute to the  
224 strong entrainment above the perturbation layer are slower cloudy updrafts and smaller  
225 distance to the cloud edge. It takes the slower cloudy updrafts (Fig. 2g) more time to  
226 traverse a given distance compared to the faster ones, which give them more time to  
227 entrain environmental air, resulting in more entrainment per unit height, an argument  
228 made previously by *Neggens et al.* [2002]. Furthermore, as less buoyant cloudy parcels  
229 get stripped away (detrained) from the outer rim of the clouds by the imposed buoyancy

230 barrier, clouds become smaller (Fig. 2i). This exposes the cloud cores to greater amounts  
 231 of entrainment.

As a representative example, Fig. 3 shows the percentage changes in updraft vertical velocity, distance to cloud edge, and stratification for parcel group 80. Changes in  $w$ ,  $d$  (distance to the cloud edge), and  $\epsilon$  are all monotonic in height, whereas changes in stratification (and the vertical gradient in cloud buoyancy) are anti-symmetric about the peak of the temperature perturbation. Changes in cloud buoyancy and environmental relative humidity take a form similar to the added temperature anomaly (but opposite in sign) and are also not consistent with changes in  $\epsilon$ . These comparisons indicate that, for the present case, changes in cloud buoyancy, vertical gradient of cloud buoyancy, and environmental relative humidity, are not of the first order importance to changes in the entrainment rates (defined in the framework of an ensemble of entraining plumes). Fig. 3d shows that relative changes in the fractional entrainment rate of a parcel group can be reproduced to a good extent by adding the relative changes in  $w$  and  $d$  with reversed signs. In other words, our result implies the following local relationship:

$$\epsilon_i = \frac{\alpha_i}{w_i d_i} \quad (1)$$

232 where the subscript  $i$  is used to highlight the fact that this relationship applies to individual  
 233 parcel groups.

234 The velocity scale  $\alpha_i$  can potentially vary among the parcel groups and heights but  
 235 remains the same with or without the temperature perturbation. Distance to the cloud  
 236 edge  $d_i$  increases below the perturbation layer and decreases above it. The decrease in  
 237  $d_i$  above the perturbation layer, as argued earlier, can be expected since the less buoyant

cloudy parcels are detrained from the outer rim of the clouds because of the buoyancy  
 barrier. The reason for the increase in  $d_i$  below the perturbation is less clear. It is possible  
 that the stronger stratification there causes the clouds to spread more horizontally, giving  
 stratification an indirect role in entrainment. But it is also possible that the increase in  
 $d_i$  is caused by changes in the convective fields below the perturbation layer during the  
 30 minute period after the imposition of the temperature anomaly. Further studies to  
 resolve this are warranted. Fig. 3d also shows that  $\delta b_i/b_i - 2\delta w_i/w_i$  does not reproduce  
 $\delta\epsilon_i/\epsilon_i$ . Therefore, the formula  $\epsilon_i \propto \frac{b}{w_i^2}$  proposed by *Gregory* [2001] in the context of a bulk  
 entraining-detraining plume model and used in an entraining plume ensemble model by  
*Chikira and Sugiyama* [2010] is not supported by the present results.

The same analyses for all higher-reaching parcel groups are shown in Fig. 4. Comparing  
 the diagnosed  $\epsilon_i$  changes from model output and calculated changes using Eq. (1), we see  
 this relationship can capture the main features of  $\epsilon_i$  changes quite well.

Based on the above suggested relationship, we calculated  $\alpha_i$  for both cases (Fig. 5).  $\alpha_i$   
 has some variations and in particular is higher close to the cloud base and for parcel groups  
 that detrain at low altitudes. This implies that, close to the cloud base, variations in  $\epsilon_i$   
 across the different parcel groups are not explained by Eq. (1). On the other hand, within  
 the bulk of the cloud layer that we examined (between 900m and 1400m),  $\alpha_i$  does not  
 vary much with height or with parcel group and takes the value of  $\sim 0.23$  m/s. The values  
 of  $\alpha_i$  also do not change much between the perturbed and control cases, consistent with  
 the inference from Figs. 3 and 4. Setting  $\alpha_i$  in Eq. (1) to 0.23 m/s reproduces model  
 diagnosed  $\epsilon_i$  over this height range quite well (results not shown here). The velocity

260 scale  $\alpha_i$  is determined entirely empirically here but may scale with the square root of  
261 the turbulent kinetic energy, as greater turbulent kinetic energy is expected to produce  
262 stronger mixing and entrainment. Such a possibility will be investigated in future studies.

263 The inverse relationship between  $\epsilon_i$  and  $w_i$  was suggested previously by *Neggers et al.*  
264 [2002] and was argued to lead to a positive feedback that amplifies the cloud-base differ-  
265 ences and produces the in-cloud heterogeneity seen in the Paluch diagram [*Paluch, 1979*].

266 The current results support the inverse relationship suggested by *Neggers et al.* [2002] but  
267 not its dominant role in explaining the in-cloud heterogeneity, which, as shown in *Krueger*  
268 *et al.* [1997], is a consequence discrete entrainment events and finite-rate turbulent mixing.

269 The inverse relationship between  $\epsilon_i$  and  $w_i$  implies that the entrainment inflow velocity  
270 (or fractional entrainment rate per unit time) is constant instead of being proportional

271 to the updraft velocity, the latter being the case in the similarity plumes of, for example,  
272 *Morton et al.* [1956]. We offer the following speculations for the possible cause of this

273 difference. In similarity plumes, turbulent mixing, vertical velocity, and buoyancy of the  
274 whole plume are tied together through the similarity relationship. In contrast, based on

275 numerical simulations of cumulus clouds, *Grabowski and Clark* [1991, 1993], for example,

276 have suggested that evaporative cooling can create a strong density gradient across the  
277 cloud-environment interface, and the interaction between the strong density gradient and

278 the shear zone across this interface is important for eddy growth, turbulent mixing, and  
279 entrainment into the clouds. Therefore, entrainment inflow velocity (or fractional entrain-

280 ment rate per unit time) in cumulus clouds may be strongly controlled by the evaporative

281 cooling and density-shear interaction across the cloud-environment boundary instead of  
282 being directly tied to the updraft velocity.

#### 4. Summary and discussions

283 We have investigated how entrainment rates of shallow cumuli depend on environmental  
284 conditions and cloud characteristics by examining their responses to a small-amplitude  
285 temperature perturbation that is horizontally uniform and localized in height. This al-  
286 lowed us to identify changes in entrainment rates associated with specific environmental  
287 conditions, while minimizing changes in other environmental conditions as well as cloud  
288 characteristics unrelated to the imposed perturbation. We analyzed the simulated cumu-  
289 lus ensemble in terms of an ensemble of entraining plumes by tracking a large number  
290 of Lagrangian parcels embedded in the LES. Partitioning cloudy updraft parcels into dif-  
291 ferent groups based on their eventual detrainment heights provided that plume ensemble  
292 view. We found that in response to the imposed warm anomaly, cloudy updraft parcels  
293 entrain slightly less in the lower portion of the perturbed layer and entrain considerably  
294 more above the peak perturbation level. Changes in the fractional entrainment rate of  
295 the  $i$ th parcel group  $\epsilon_i$  are quite well described by a simple inverse relationship between  
296  $\epsilon_i$  and the vertical velocity  $w_i$  and the distance to the cloud edge of that parcel group  
297 (Eq. (1)). The proportionality factor  $\alpha_i$ , tentatively interpreted as a turbulent velocity  
298 scale, is nearly constant ( $\sim 0.23\text{m/s}$ ) over the bulk of the cloud layer (900-1400m). In  
299 addition,  $\alpha_i$  does not differ much between the control and perturbed cases, and setting  
300 it to  $0.23\text{m/s}$  seems to reproduce entrainment rates quite well over the bulk of the cloud  
301 layer in this shallow convection case (BOMEX). While our analyses and results are for an



302 ensemble of entraining plumes, the entraining plume ensembles can be combined to give  
303 a bulk entraining-detraining plume [see e.g. *Lawrence and Rasch*, 2005].

304 A major emphasis of this paper is to describe our Lagrangian tracking-based analysis  
305 of linear response functions of convection and to illustrate its value in gaining insight  
306 into the underlying dynamics. To that end, we have focused on the effects of an imposed  
307 temperature perturbation, which emphasizes certain aspects of convection because of its  
308 effect as a buoyancy barrier. Imposing other types of perturbations may allow tests that  
309 are better tailored to other aspects of the convection. For example, a small-amplitude  
310 moisture perturbation that is horizontally uniform and localized in height may allow a  
311 closer analysis of the effect of environmental relative humidity with less influence from  
312 the buoyancy barrier effect. Such additional experiments could be valuable, although we  
313 do note that responses to such a moisture anomaly have been found to be weak in the  
314 BOMEX case [*Nie and Kuang*, 2012a]. Since analyses and results in the present paper are  
315 based on the specific case of BOMEX, studies of additional cases are clearly warranted to  
316 generalize the results.

317 Some aspects of the present simulations shall be improved in future studies. As the  
318 typical effective radius of the simulated clouds is 150 to 200m (see Supplementary Infor-  
319 mation), the numerical resolution used in this study ( $dx=dy=50m$ ,  $dz=25m$ ), while finer  
320 than that adopted in the BOMEX LES intercomparison study of *Siebesma et al.* [2003]  
321 ( $dx=dy=100m$  and  $z=40m$ ), does not resolve most of the entraining eddies across the  
322 cloud-environment interface. Entrainment in the simulations therefore depends on the  
323 SGS closure and does not account for SGS heterogeneity in mixing, leaving open the

324 possibility of too-rapid SGS mixing and evaporation. *Nie and Kuang* [2012a, b], using  
325 the SAM model, found that the linear response functions and the mixing characteristics  
326 of the BOMEX case were robust when resolutions were varied from  $dx=dy=dz=25m$  to  
327  $dx=dy=100m, dz=50m$ . While that lends some confidence to our results, it is desirable to  
328 repeat our simulations and analyses using higher resolutions in future studies so that the  
329 entraining eddies can be better resolved. In addition to numerical resolution, *Jarecka et*  
330 *al.* [2009, 2013] also explored more sophisticated SGS closures to account for the hetero-  
331 geneity of SGS mixing and found that, with resolution similar to that used in the present  
332 study, the effect of the more sophisticated SGS closures is somewhat limited, and the  
333 effect of heterogeneity in SGS mixing is small. *Jarecka et al.* [2013] argued that the latter  
334 is because the environmental air entrained into trade cumuli is already close to saturation  
335 (in contrast to the case of stratocumulus). However, it is not yet clear whether their SGS  
336 closures are adequate, and combining an approach such as the linear eddy model (*Krueger*  
337 *et al.* [1997]) and the LES may be necessary to more fully address the issue of SGS mixing  
338 and evaporation. As noted in sections 2 and 3, there is also some drift in the horizontally  
339 averaged sounding over the 30 minute period that we analyze (Fig. 1), complicating the  
340 interpretation. Future studies will employ time-invariant forcings to minimize such drifts.  
341 Lastly, we note that the same methodology can be applied to deep convection and the  
342 results will be reported in a forthcoming publication.

343 **Acknowledgments.** This research was partially supported by the Office of Biological  
344 and Environmental Research of the U.S. DOE under grant DE-SC0008679 as part of  
345 the ASR Program, NOAA grant NA13OAR4310154, and NSF grant AGS-1260380. The

346 authors thank Marat Khairoutdinov for making the SAM model available, Martin Singh,  
347 Giuseppe Torri, Pedram Hassanzadeh for valuable comments, and Steve Krueger, Roel  
348 Neggers for very helpful reviews. The Harvard Odyssey cluster provided much of the  
349 computing resources for this study.

## Notes

1. Unless specified otherwise, fractional entrainment rate throughout this paper refers to fractional entrainment rate per  
350 unit height.

## References

- 351 Arakawa, A. and W.H. Schubert (1974), *Interaction of a cumulus cloud ensemble with the*  
352 *large-scale environment. Part I, J. Atmos. Sci., 31, 674-701.*
- 353 Bechtold, P., M. Kohler, T. Jung, F. Doblas-Reyes, M. Leutbecher, M. J. Rodwell, F.  
354 Vitart and G. Balsamo (2008), *Advances in simulating atmospheric variability with the*  
355 *ECMWF model: From synoptic to decadal time-scales. Q. J. R. Meteorol. Soc., 34,*  
356 *1337-1351.*
- 357 Bretherton, C. S. and P.K. Smolarkiewicz (1989), *Gravity Waves, compensating subsi-*  
358 *dence, and detrainment around cumulus clouds, J. Atmos. Sci., 46, 740-759.*
- 359 Bretherton, C. S., J. R. McCAA, and H. Grenier (2004), *A new parameterization for shal-*  
360 *low cumulus convection and its application to marine subtropical cloud-topped boundary*  
361 *layers. Part I: Description and 1D results. Mon. Wea. Rev., 132, 864-882.*
- 362 Chikira, M. and M. Sugiyama (2010), *A cumulus parameterization with state-dependent*  
363 *entrainment rate. part i: description and sensitivity to temperature and humidity pro-*  
364 *files. J. Atmos. Sci., 67, 2171-2193.*

- 365 Dawe, J. T. and P.H. Austin (2013), *Direct entrainment and detrainment rate distributions*  
366 *of individual shallow cumulus clouds in an LES. Atmos. Chem. Phys.*, 13, 7795-7811.
- 367 Emanuel, K. A. and M. Zivkovic-Rothman (1999), *Development and Evaluation of a*  
368 *Convection Scheme for Use in Climate Models. J. Atmos. Sci.*, 56, 1766-1782.
- 369 Grabowski, W. W. and T. L. Clark (1991), *Cloud-Environment Interface Instability: Ris-*  
370 *ing Thermal Calculations in Two Spatial Dimensions. J. Atmos. Sci.*, 48, 527-546.
- 371 Grabowski, W. W. and T. L. Clark (1993), *Cloud-Environment Interface Instability: Part*  
372 *II: Extension to Three Spatial Dimensions. J. Atmos. Sci.*, 50, 555-573.
- 373 Grant, A.L.M and A. R. Brown (1999), *A similarity hypothesis for shallow-cumulus trans-*  
374 *ports. Q. J. R. Meteorol. Soc.*, 125, 1913-1936.
- 375 Gregory, D. (2001), *Estimation of entrainment rate in simple models of convective clouds.*  
376 *Q. J. R. Meteorol. Soc.*, 127, 53-72.
- 377 Hohenegger, C. and C. S. Bretherton (2011), *Simulating deep convection with a shallow*  
378 *convection scheme., Atmos. Chem. Phys.*, 11, 10389-10406.
- 379 Heus, T. (2008), *Mixing in shallow cumulus clouds studied by lagrangian particle tracking.,*  
380 *J. Atmos. Sci.*, 65, 2581-2597.
- 381 Holland, J. Z. and E. M. Rasmusson (1973), *Measurement of atmospheric mass, energy,*  
382 *and momentum budgets over a 500-kilometer square of tropical ocean., Mon. Wea. Rev.*,  
383 *101*, 44-55.
- 384 Jarecka, D., W. W. Grabowski, and H. Pawlowska (2009), *Modeling of subgrid-scale mixing*  
385 *in large-eddy simulation of shallow convection., J. Atmos. Sci.*, 66, 2125-2133.

- 386 Jarecka, D., W. W. Grabowski, and H. Pawlowska (2013), *Homogeneity of the subgrid-*  
387 *scale turbulent mixing in large-eddy simulation of shallow convection.*, *J. Atmos. Sci.*,  
388 *70*, 2751-2767.
- 389 Krueger, S. K., C.-W. Su, and P. A. McMurtry (1997), *Modeling entrainment and fine-*  
390 *scale mixing in cumulus clouds.*, *J. Atmos. Sci.*, *54*, 2697-2712.
- 391 Kuang, Z. and S.C. Bretherton (2006), *A mass-flux scheme view of a high-resolution*  
392 *simulation of a transition from shallow to deep cumulus convection.*, *J. Atmos. Sci.*, *63*,  
393 1895-1909.
- 394 Kuang, Z. (2010), *Linear response functions of a cumulus ensemble to temperature and*  
395 *moisture perturbations and implication to the dynamics of convectively coupled waves.*,  
396 *J. Atmos. Sci.*, *67*, 941-962.
- 397 Kuang, Z. (2012), *Weakly Forced Mock Walker Cells.*, *J. Atmos. Sci.*, *69*, 2759-2786.
- 398 Khairoutdinov, M. F. and D. A. Randall (2001), *A cloud-resolving model as a cloud*  
399 *parameterization in the NCAR Community Climate System Model: Preliminary results,*  
400 *Geophys. Res. Lett.*, *28*, 3617-3620.
- 401 Lawrence M. G. and P. J. Rasch (2005), *Tracer Transport in Deep Convective Updrafts:*  
402 *Plume Ensemble versus Bulk Formulations.* *J. Atmos. Sci.*, *62*, 2880-2894.
- 403 Lin, C. and A. Arakawa (1997), *The macroscopic entrainment processes of simulated*  
404 *cumulus ensemble. part II: Testing the entraining-plume model.*, *J. Atmos. Sci.*, *54*,  
405 1044-1053.
- 406 Lin, C. (1999), *Some bulk properties of cumulus ensembles simulated by a cloud-resolving*  
407 *model. part II: Entrainment profiles,* *J. Atmos. Sci.*, *56*, 3736-3748.

- 408 Mapes, B and R. Neale (2011), *Parameterizing convective organization to es-*  
409 *cape the entrainment dilemma. J. Adv. Model. Earth Syst., 3, M06004,*  
410 *DOI:10.1029/2011MS000042.*
- 411 Morton, B., Taylor, G. and Turner, J. (1956), *Turbulent gravitational convection from*  
412 *maintained and instantaneous sources Proc. Roy. Soc. London., 234, 1- 23.*
- 413 Neggers, R. A. J, A. P. Siebesma, and H.J.J. Jonker (2002), *A multipacel model for shallow*  
414 *cumulus convection. J. Atmos. Sci., 59, 1655-1668.*
- 415 Nie, J. and Z. Kuang (2012a), *Responses of shallow cumulus convection to large-scale*  
416 *temperature and moisture perturbations: A comparison of large-eddy simulations and a*  
417 *convective parameterization based on stochastically entraining parcels., J. Atmos. Sci.,*  
418 *69, 1936-1956.*
- 419 Nie, J. and Z. Kuang (2012b), *Beyond bulk entrainment and detrainment rates: a new*  
420 *frame- work for diagnosing mixing in cumulus convection, Geophys. Res. Lett., 39,*  
421 *L21803, doi:10.1029/2012GL053992.*
- 422 Paluch, I. R. (1979), *The entrainment mechanism in Colorado cumuli., J. Atmos. Sci.,*  
423 *36, 2467-2478.*
- 424 Raymond D. J. and A. M. Blyth, (1986), *A Stochastic Mixing Model for Nonprecipitating*  
425 *Cumulus Clouds., J. Atmos. Sci., 43, 2708-2718.*
- 426 Romps, D.M. and Z. Kuang (2010), *Do undiluted convective plumes exist in the upper*  
427 *tropical troposphere?, J. Atmos. Sci., 67, 468-484.*
- 428 Romps, D.M. (2010), *A direct measure of entrainment, J. Atmos. Sci., 67, 1908-1927.*

- 429 Siebesma, A.P. (1998), *Shallow cumulus convection.*, in *Buoyant Convection in Geophys-*  
430 *ical Flows*, E. J. Plate, et al., Eds., Kluwer Academic, 441-486.
- 431 Siebesma, A.P., C.S. Bretherton, A. Brown, A. Chlond, J. Cuxart, P.G. Duynkerke, H.  
432 Jiang, M. Khairoutdinov, D. Lewellen, C-H. Moeng, E. Sachedz, B. Stevens, and D.E.  
433 Stevens (2003), *A large eddy simulation inter comparison study of shallow cumulus*  
434 *convection J. Atmos. Sci.*, 60 1201-1219.
- 435 Simpson, J. and V. Wiggert (1969), *Models of precipitating cumulus towers*, *Mon. Wea.*  
436 *Rev.*, 97, 471-489.
- 437 Tiedtke, M. (1989), *A comprehensive mass flux scheme for cumulus parameterization in*  
438 *large-scale models Mon. Wea. Rev.*, 117, 1779-1800.
- 439 Torri, G., Z. Kuang, and Y. Tian (2015), *Mechanisms for convection triggering by cold*  
440 *pools. Geophys. Res. Lett.*, 42, 1943-1950.
- 441 Weil, J. C. (2004), *The use of large-eddy simulation in lagrangian particle dispersion*  
442 *models, J. Atmos. Sci.*, 61, 2877-2887.
- 443 Yeo, K. and D. Romps (2013), *Measurement of convective entrainment using lagrangian*  
444 *particles.*, *J. Atmos. Sci.*, 70, 266-277.

445

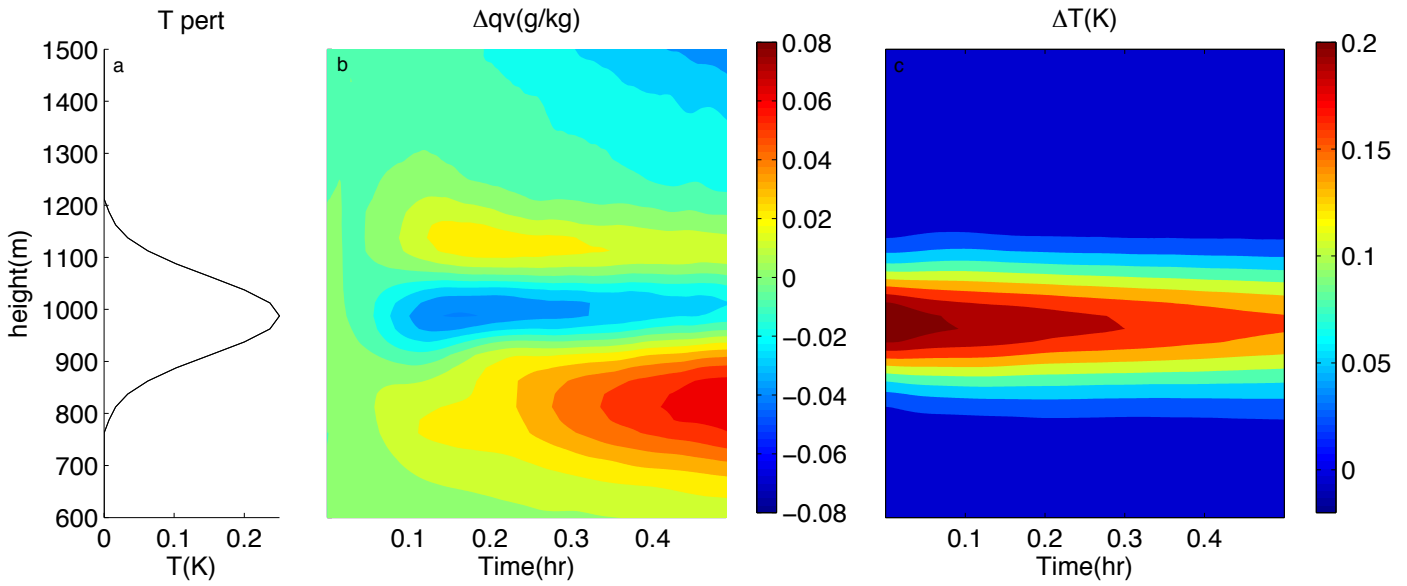


**Figure 1.** (a) Initial temperature perturbation profile, (b) horizontally averaged moisture anomalies as a function of height and time, (c) same as (b) but for temperature.



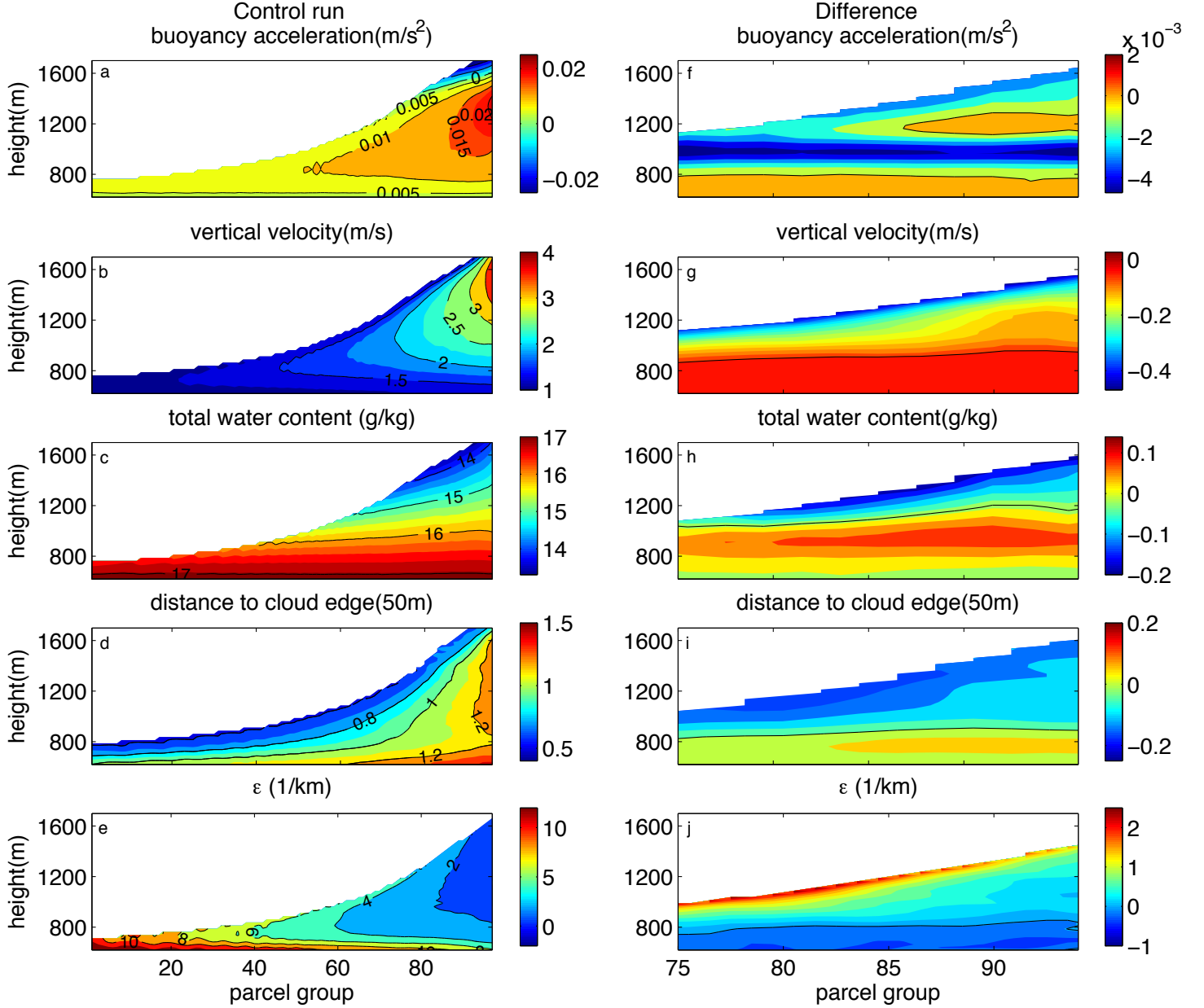


**Figure 2.** (Left column) control run cloudy updraft (a) buoyancy acceleration, (b) vertical velocity, (c) total water content, (d) distance to the cloud edge (with the unit of grid spacing), (e) fractional entrainment rate  $\epsilon$  per km, as functions of parcel group and height (see text for details on how the parcel groups are defined); (right) the same as the left column but for the differences between the ensemble perturbed and control runs.

Solid black curve delineates the zero contour line.

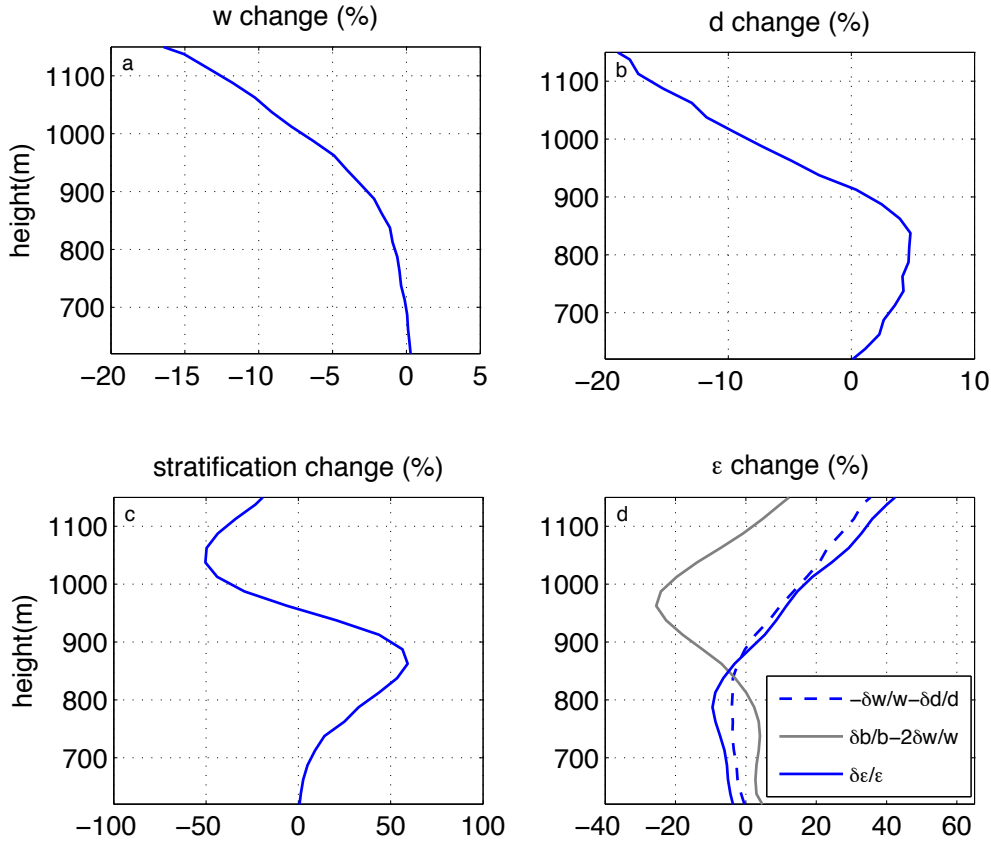


**Figure 3.** Percentage change in (a) vertical velocity ( $w$ ), (b) distance to the cloud edge ( $d$ ), (c) stratification, and (d) fractional entrainment rate ( $\epsilon$ ) for parcel group 80. The sum of the percentage changes in vertical velocity and distance to cloud edge with the sign reversed is also plotted in (d), the gray line denotes the sum of the percentage changes in buoyancy and vertical velocity, which corresponds to the empirical relation proposed by Gregory [2001]. Stratification is calculated as  $d\theta_\rho/dz$ ,  $\theta_\rho$  is the density potential temperature which takes into account water loading in calculating parcel densities. Distance to the cloud edge is calculated as the minimum distance to the cloud edge.

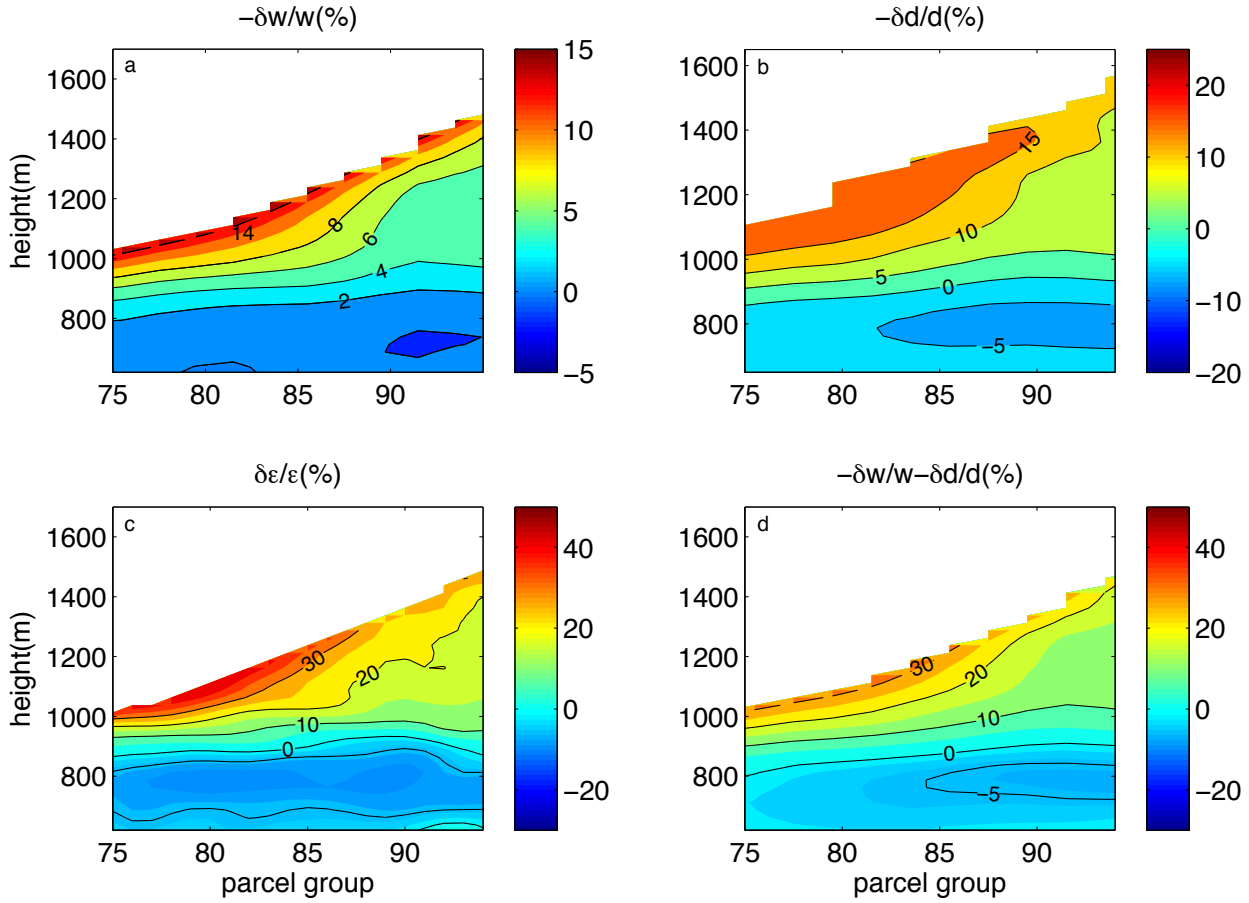


**Figure 4.** Percentage change in (a) vertical velocity, (b) distance to cloud edge, and (c) fractional entrainment rate  $\epsilon$  diagnosed from the model,. The sum of the percentage changes in vertical velocity and in distance to cloud edge with the sign reversed, is shown in (d).

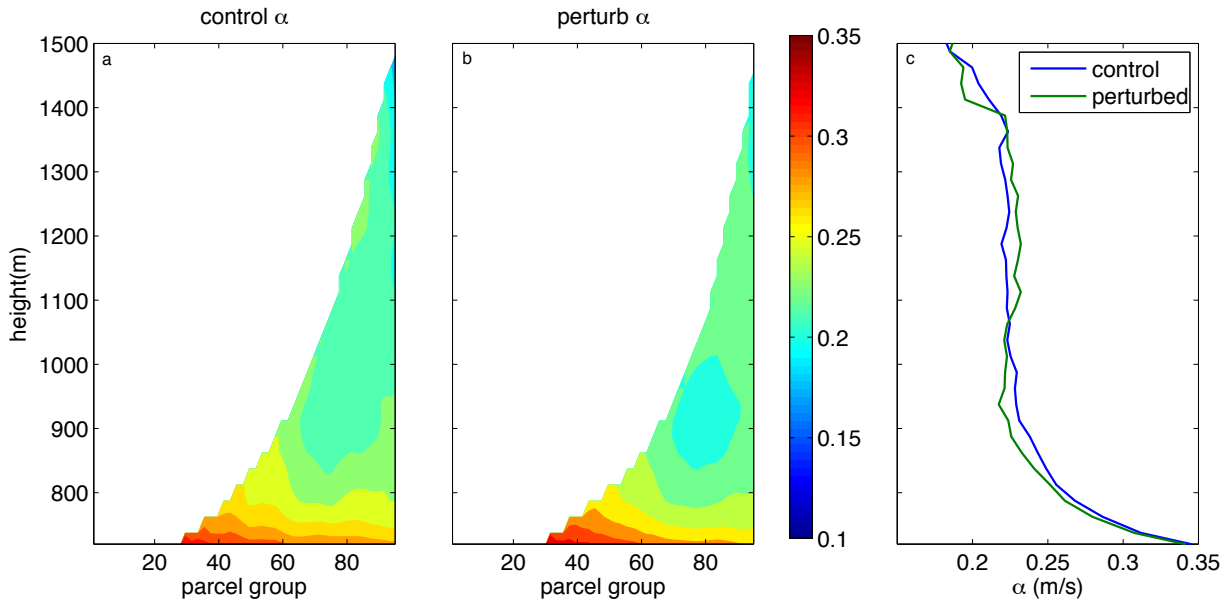


**Figure 5.** (a) Coefficients  $\alpha$  determined from Eq. (1) using  $\epsilon$ ,  $w$ , and distance to the cloud edge diagnosed from the control runs, (b) same as (a) but for the perturbed runs, (c)  $\alpha$  values averaged across all parcel groups as a function of height.